Influence of Interface Textures on Light Management in Thin-Film Silicon Solar Cells With Intermediate Reflector

Chao Zhang, Matthias Meier, André Hoffmann, Wendi Zhang, Karsten Bittkau, Gabrielle Jost, Ulrich W. Paetzold, Markus Ermes, and Tsvetelina Merdzhanova

***Abstract*—High-efficiency thin-film silicon solar cells require advanced textures at the front contacts for light management. In this contribution, the influence of the texture of various transparent conductive oxides (TCO) on the effectiveness of an intermediate reflector layer (IRL) in a-Si:H/μc-Si:H tandem solar cells is investigated. The employed front side TCOs include several types of sputter-etched ZnO:Al, LPCVD ZnO:B and APCVD SnO_2:F. The topographies after different stages of the deposition process of the tandem solar cell, at the front TCO, after deposition of the amorphous top cell and after the deposition of the microcrystalline bottom cell, were characterized by atomic force microscopy at precisely the same spot. The external quantum efficiency of the fabricated solar cells were measured and successfully reproduced by a finite-difference time-domain method applying the measured topographies at each interface of the solar cell. With these simulations, the impact of structure type and feature size on the effectiveness of the IRL is investigated. The highest IRL effectiveness in a tandem solar cell was found for double-textured ZnO:Al. In this contribution, we study the interplay between interface textures and parasitic losses. Our findings are relevant for the design of topography for optimized IRL performance.**

***Index Terms*—A-Si:H/μc-Si:H, finite-difference time-domain (FDTD) simulation, intermediate reflector layer, light management, silicon tandem solar cell, transparent conductive oxides (TCO).**

I. Introduction

THIN-FILM silicon tandem solar cells based on a hydrogenated amorphous (a-Si:H) top and a microcrystalline (μc-Si:H) bottom cell are well investigated and an industrially applied technology. A challenge of this type of solar cells is the light-induced degradation of a-Si:H material and the associated deterioration of the electrical properties known as the Staebler–Wronski effect [1]. To minimize the resulting efficiency loss, it is beneficial to reduce the thickness of the a-Si:H top cell [2]. Since both subcells are connected in series, the subcell with the lowest current density limits the total current density of the whole device. A strategy to maintain a high current density, even with thinner top cell absorber layers, is to introduce an intermediate reflector layer (IRL) made of microcrystalline silicon oxide (μc-SiO_x:H) between the top and bottom cell [3]–[7]. This additional layer has a lower refractive index compared with silicon and reflects a part of the incident light back into the top cell. Thereby, the current of the top cell and the bottom cell can be matched despite the reduced thickness of the a-Si:H top solar cell. A lot of study has been accomplished on the texture and thickness related effectiveness of an IRL. Detailed investigations have been made applying periodic [8] and randomly textured interfaces [9]–[14]. Some precise predictions on the impact of a thickness variation of the IRL on the top and bottom cell current focusing on the low pressure chemical vapor deposition (LPCVD) ZnO:B texture are shown in [12]. While other groups focused on finding an optimal thickness of the IRL and its impact on light kept in the top cell, the emphasis in our contribution is on the impact of a large range of different textures applying only one single thickness for the IRL on all samples.

The correlation between solar cell topography and short-circuit current density by investigating tandem silicon solar cells with and without IRL fabricated on eight different front textures is discussed. A series of electromagnetic simulations based on atomic force microscopy (AFM) measurements of the interfaces taken from these devices after different stages of the production were also performed. The optical simulations over a wide wavelength range allow a detailed study of computed modified textures. They make it possible to go beyond experimental limitations and investigate parasitic losses that occur in tandem cell devices.

II. Experimental Details

All solar cells were fabricated using an RF-PECVD system (30×30 cm^2; 13.56 MHz) suitable for eight 5×10 cm^2 substrates. This way, the solar cells were processed at the same deposition conditions. The process gases used were silane (SiH_4) and hydrogen (H_2). For p-type layers, we used trimethylborane [$B(CH_3)_3$] and for the n-type material phosphine (PH_3) was added. CO_2 was used as an oxygen source for the n-type μc-SiO_x:H intermediate reflector layer. The gases were applied to the process through a showerhead electrode. More details are given elsewhere [15]. The fabricated tandem cells contain a 300-nm-thick a-Si:H top cell and a 1500-nm-thick μc-Si:H bottom cell. They were prepared with and without an IRL made of

Manuscript received July 10, 2014; revised October 14, 2014; accepted October 14, 2014. Date of publication November 20, 2014; date of current version December 18, 2014. This work was supported by the FP7 Project "Fast Track," funded by the EC under Grant 283501. The FDTD simulations were performed at Jülich Supercomputing Center under the VSR Project JIPV00.

The authors are with the Am Institut für Energie- und Klimaforschung-Photovoltaik, Forschungszentrum Jülich GmbH, 52425 Jülich, Germany (e-mail: c.zhang@fz-juelich.de; ma.meier@fz-juelich.de; a.hoffmann@fz-juelich.de; mail@zhangwendi.com; k.bittkau@fz-juelich.de; g.jost@fz-juelich.de; u.paetzold@fz-juelich.de; m.ermes@fz-juelich.de; t.merdzhanova@fz-juelich.de).

Color versions of one or more of the figures in this paper are available online at http://ieeexplore.ieee.org.

Digital Object Identifier 10.1109/JPHOTOV.2014.2364399

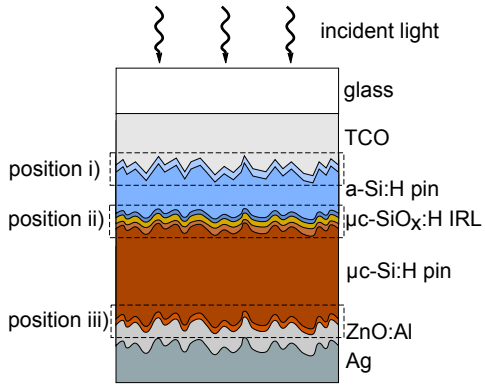

Fig. 1. Schematic of an a-Si:H/μc-Si:H tandem solar cell with marked positions at which characterizations were carried out.

TABLE I
LIST OF TRANSPARENT CONDUCTIVE OXIDES FRONT CONTACTS

type	TCO material	remark	*ACL*, nm	σ_{RMS},nm
A	ZnO:Al (1%)	35 s HCl	715	110
B	ZnO:Al (1%)	20 s HF / 10 s HCl	470	80
C	ZnO:Al (0.5%)	90 s HCl / 20 s HF	380	70
D	ZnO:Al (0.5%)	90 s HCl etched	855	125
E	ZnO:Al (0.5%)	120 s HCl etched	1110	160
F	ZnO:B	LPCVD	290	80
G	SnO_2:F	AGC	190	35
H	ZnO:Al (1%)	flat	5	5

n-type μc-SiO_x:H (refractive index $n = 2.5$). The IRL is 70 nm thick. A schematic drawing of a tandem solar cell with IRL is shown in Fig. 1.

The types of employed transparent conductive oxides (TCO) front contacts are: sputtered ZnO:Al [16], LPCVD ZnO:B from EPFL in Neuchâtel [17] and atmospheric pressure chemical vapor deposition SnO_2:F coated glass from *Asahi Glass Company* (AGC). Two different targets were used for the sputtered ZnO:Al containing 1% and 0.5% aluminum. Sputtered ZnO:Al substrates were etched in 0.5 w/w% HCl and 1 w/w% HF [18] with varied etching time. The autocorrelation length (*ACL),* a parameter to describe the lateral size of surface features, and the root mean square roughness (σ_{RMS}) are derived from AFM measurements. The details are shown in Table I.

The topographies of the samples at precisely the same spot were characterized by AFM after different stages of the fabrication process. The stages are shown in Fig. 1. Those are: 1) at the front TCO, 2) after the deposition of the a-Si:H top cell, and 3) after the deposition of the μc-Si:H bottom cell. The AFM measurements were conducted with a Nanostation 300 SIS system with a resolution of 1024×1024 pixel for an area of 20×20 μm^2. For the determination of the photovoltaic parameters and the external quantum efficiency (*EQE)*, the solar cells were processed in a separate run. Solar cells deposited on ZnO front contacts included an additional p-type μc-Si:H contact layer, while the solar cells deposited on SnO_2:F only contain a p-type a-SiC:H layer. *J–V* measurements were conducted in a class A sun simulator. *EQE* measurements were performed to calculate the top and bottom cell current density ($J_{\mathrm{EQE,top}}$, $J_{\mathrm{EQE,bot}}$). The reflectance *R* was measured using a UV-VIS-NIR Perkin-Elmer photo spectrometer with integrating sphere.

The AFM data gained for each interface texture served as input parameter for the finite-difference time-domain (FDTD) simulations that solve Maxwell's equations rigorously. The FDTD method uses a home-built interface to the software package *Meep* [19]. The calculation domain has a lateral size of 4.3×4.3 μm^2 and the grid size is 10 nm. The simulations consider a planar incident electromagnetic wave at normal incidence and cover a spectrum from 500 to 1050 nm in 50-nm steps. The layer stack consists of a glass half space with a refractive index of 1.5, a front contact layer (TCO), an a-Si:H slab with a thickness of 300 nm, an IRL followed by a μc-Si:H slab with a thickness of 1500 nm, and a ZnO:Al/silver back reflector. Due to convergence purposes of the rigorous simulation, the silver was replaced by a perfect electric conductor. The optical constants of the front contact layers were assumed for all cases to be the ones of ZnO:Al. The refractive indices and absorption coefficients for the ZnO:Al, a-Si:H and μc-Si:H were determined by reflection/transmission measurements and photothermal deflection spectroscopy. The glass/ZnO:Al interface was assumed to be flat while all other interfaces were textured using topographies from AFM measurements for interlayer textures at positions i), ii) and iii). More details on the simulation method are given elsewhere [20].

III. RESULTS AND DISCUSSION

A. Effect of Interface Textures on Intermediate Reflector Layer Performance

AFM scans were performed on every TCO at three positions in the tandem solar cell. The evolution of the topography from the front to the bottom texture for type A, C, F, and G TCO is shown in Fig. 2 as an example.

The type A TCO represents a state-of-the-art sputter-etched single-textured ZnO:Al with crater-like features. In general, the topography is relatively flat and contains large features. Type B TCO, with AFM data not shown, reveals a slightly steeper crater like structure compared with type A. In addition, the *ACL* is significantly smaller (470 nm). Type C TCO, on the other hand, is a sputter-etched double-textured ZnO:Al with enhanced light scattering properties [21]. Here, an additional HF etching step for 20 s was performed subsequently after the HCl etching, which results in the formation of steep etch-pits in submicrometer-size. Type D TCO (90 s HCl-etched ZnO:Al) and type E TCO (120 s HCl etched) show a similar texture compared with type A and B but with larger features. The *ACL* is 855 and 1110 nm, respectively. Especially for type E TCO, a flatter texture with an angular distribution shifted to lower angles is observed. The features include additional smaller and steeper structures than in the case of type A. The texture of type F TCO consists of steep pyramids with an *ACL* of 290 nm. For type G TCO, flatter and smaller pyramids are seen. Generally, the sharp edges which are visible on the bare TCO in Fig. 2, position i) are smoothened after the deposition of the amorphous silicon top cell [see Fig. 2, position ii)]. The AFM images also indicate

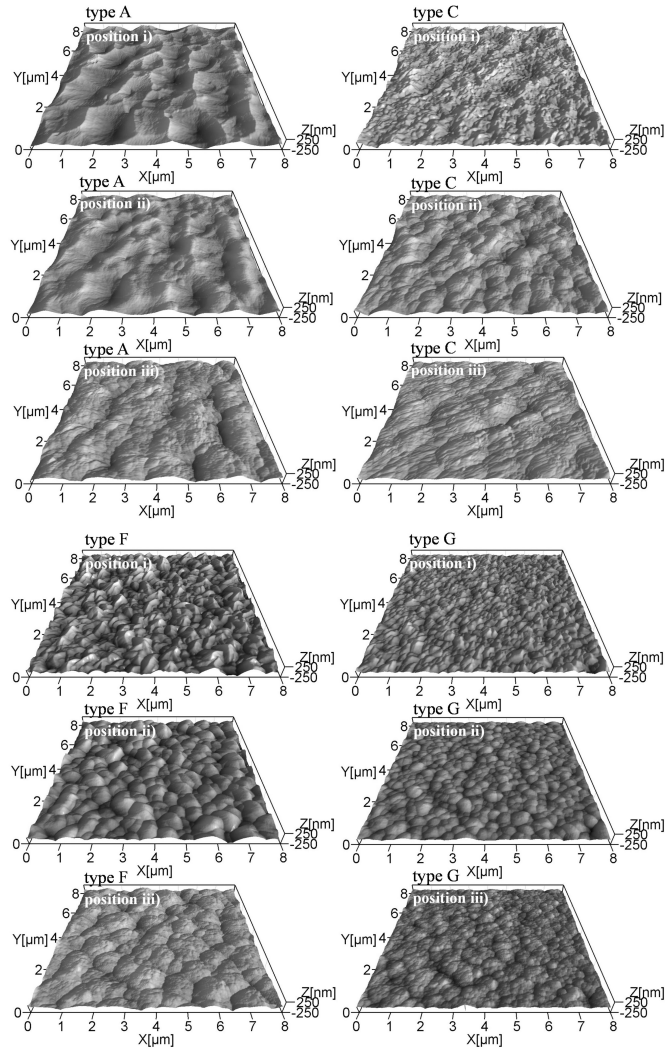

Fig. 2. AFM images measured after different stages of the deposition of tandem solar cells on type A, C, F and G front TCO. i) Front TCO texture. ii) a-Si:H top cell texture. iii) μc-Si:H bottom cell texture. The measurements are taken at each sample for exactly the same area.

that the surface topography of the growth model described in [22] sufficiently matches the measured topography after the a-Si:H growth. A nonconformal growth is observed, while the morphology of the back side shows additional substructures that occurs with a μc-Si:H growth [see Fig. 2, position iii)]. As a parameter for the texture *ACL* and root mean square roughness (σ_{RMS}) are derived from these AFM data.

In Table II, the photovoltaic parameters of tandem cells with and without IRL deposited on various front textures are listed. In addition, $J_{\mathrm{EQE,top}}$ and $J_{\mathrm{EQE,bot}}$ from *EQE* measurements are presented. It is seen that the top and the bottom cell current densities show large differences when comparing solar cells deposited on different front textures. This is driven by a different light scattering of incident light at each texture. The efficiencies of the tandem cells vary from 8.3% for flat ZnO:Al (type H) to 11.8% for ZnO:B (type F). With exception of the flat front contact (type H), the tandem cells are limited by the top cell, and therefore, the introduction of an IRL leads to an improvement of efficiencies.

TABLE II
J–V PARAMETER AND J_{EQE} OF TANDEM CELL DEPOSITED ON VARIOUS TRANSPARENT CONDUCTIVE OXIDES, WITH AND WITHOUT INTERMEDIATE REFLECTOR LAYER

without IRL							
type	η [%]	*FF* [%]	V_{OC} [V]	J_{SC} [mA/cm^2]	$J_{\mathrm{EQE,top}}$ [mA/cm^2]	$J_{\mathrm{EQE,bottom}}$ [mA/cm^2]	$J_{\mathrm{EQE,total}}$ [mA/cm^2]
A	10.4	71.4	1.37	10.6	10.4	14.1	24.5
B	10.2	71.7	1.37	10.4	10.4	13.6	24.0
C	11.1	73.8	1.34	11.2	11.0	13.8	24.8
D	10.1	71.6	1.39	10.1	10.0	12.4	22.4
E	10.4	71.6	1.37	10.6	10.3	13.8	24.2
F	11.3	74.4	1.36	11.2	11.2	14.2	25.4
G	11.0	73.7	1.35	11.0	11.0	11.5	22.5
H	8.8	73.9	1.38	8.6	9.5	8.1	17.6
with IRL							
type	η [%]	*FF* [%]	V_{OC} [V]	J_{SC} [mA/cm^2]	$J_{\mathrm{EQE,top}}$ [mA/cm^2]	$J_{\mathrm{EQE,bottom}}$ [mA/cm^2]	$J_{\mathrm{EQE,total}}$ [mA/cm^2]
A	10.9	71.1	1.38	11.2	11.0	12.2	23.2
B	10.7	70.7	1.36	11.1	11.1	12.0	23.1
C	11.4	71.6	1.33	11.9	12.1	12.2	24.3
D	10.4	72.4	1.38	10.4	10.1	10.8	20.9
E	10.6	71.7	1.38	10.8	10.7	11.1	21.8
F	11.8	72.3	1.36	12.0	12.2	12.3	24.5
G	10.4	79.9	1.34	9.7	12.1	9.50	21.6
H	8.3	81.1	1.37	7.5	9.6	7.0	16.6

In Fig. 3(a) and (b), the *EQE* and absorptance (*1-R*) of tandem solar cells deposited on type A and type C TCO are compared as an example of poor and high IRL performance.

The increase of generated charge carriers in the top cell ($J_{\mathrm{EQE,top}}$-gain) and the decrease in the bottom cell ($J_{\mathrm{EQE,bot}}$-loss) strongly depend on the type of front texture. With IRL, the $J_{\mathrm{EQE,top}}$ of the solar cell deposited on type A TCO was increased by 0.6 mA/cm^2, while the $J_{\mathrm{EQE,bot}}$ was decreased by 1.9 mA/cm^2. In contrast, $J_{\mathrm{EQE,top}}$ for a solar cell deposited on type C TCO was increased by 1.1 mA/cm^2, and $J_{\mathrm{EQE,bot}}$ was decreased by 1.6 mA/cm^2. The additional cell reflectance due to an IRL is more pronounced for tandem cells deposited on type A compared with type C TCO. Furthermore, it is supposed that a part of the light, which is reflected back into the top cell and not been fully absorbed in the silicon, might be absorbed in the TCO when passing it for the second time. This effect also seems to be larger in the case of type A TCO when comparing the discrepancy between the cell reflectance and the total *EQE*. The pronounced interference effects seen for type A are reduced in the case of the double-textured ZnO:Al (type C).

ΔJ_{EQE} indicates parasitic loss due to an additional IRL. It is defined as the difference of the total current density between a tandem solar cell with and without an IRL and amounts to –1.3 mA/cm^2 in the case of type A and –0.5 mA/cm^2 for type C TCO. Altogether, these parameters describe the effectiveness of an IRL.

Fig. 4 (a) shows the correlation between the current improvement in the top cell ($J_{\mathrm{EQE,top}}$-gain) versus the *ACL* of various TCO front textures. It is seen that especially small *ACL*s of textured TCOs are linked to large improvements. In Fig. 4(b), *EQE* results of tandem solar cells with IRL deposited on

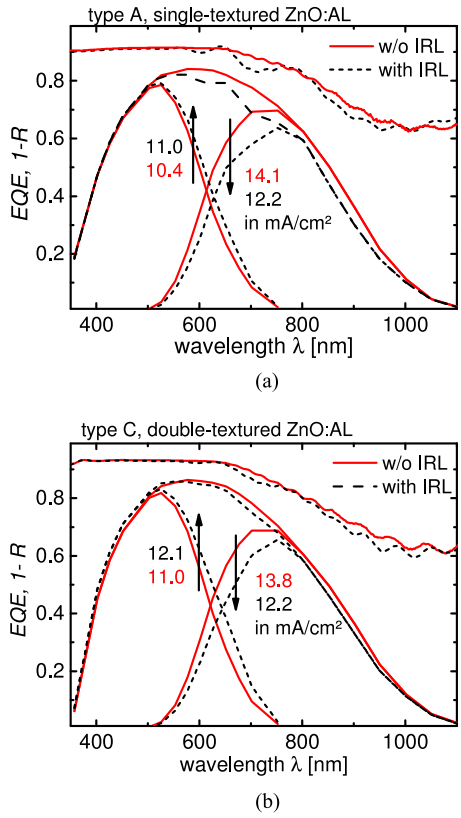

Fig. 3. *EQE* and absorptance (*1-R*) of tandem solar cells deposited on (a) type A TCO and (b) type C TCO. Dashed black lines show *EQE* of solar cells deposited with and solid red lines without IRL. Current densities ($J_{\mathrm{EQE,top}}$, $J_{\mathrm{EQE,bot}}$) were calculated from *EQE* measurements for solar cells with and without IRL.

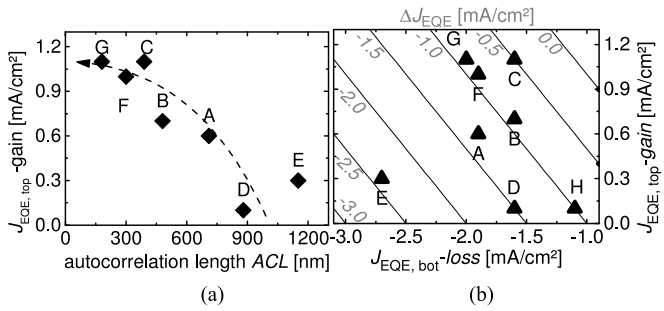

Fig. 4. (a) $J_{\mathrm{EQE,top}}$-gain plotted against *ACL* of TCO front textures. The dashed arrow is a guide to the eye. (b) Increase of the top current ($J_{\mathrm{EQE,top}}$-gain) as a function of decrease of bottom current ($J_{\mathrm{EQE,bot}}$-loss) of tandem solar cells caused by an additional IRL deposited on various TCOs. Constant ΔJ_{EQE} is shown in diagonal lines.

various TCOs compared with solar cells without IRL are presented. The $J_{\mathrm{EQE,top}}$-gain is plotted against the reduction of the bottom cell current density ($J_{\mathrm{EQE,bot}}$-loss). Constant ΔJ_{EQE} ($\Delta J_{\mathrm{EQE}} = J_{\mathrm{EQE,top}}$-gain + $J_{\mathrm{EQE,bot}}$-loss) values are included as diagonal lines. It is seen that the IRL effectiveness for tandem solar cells deposited on type C TCO (double textured) is by far the highest compared with all other textures. The highest efficiencies, as well as the highest total currents, are found for type F TCO, closely followed by type C. Even though type C TCO showed a higher effectiveness of the IRL, it has

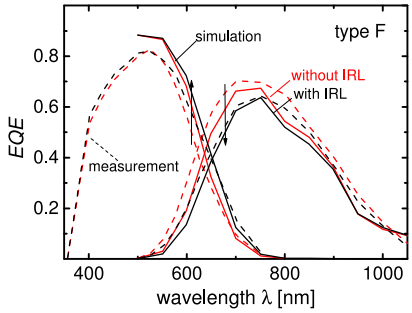

Fig. 5. FDTD simulations of *EQE* shown as solid lines. The black curves represent the *EQE* of a tandem solar cell with and the red curves without an IRL. As a reference, the measured *EQE* of a tandem solar cell with IRL is shown as dashed lines. The employed interface textures are from type F TCO (LPCVD ZnO:B).

been outperformed in terms of top and bottom cell current densities for both cases, with and without an IRL. Nevertheless, it has been shown that its texture makes it possible to improve the ΔJ_{EQE} significantly, which is attributed to the small and very steep craters created by an HF etching step. For types D and E (large craters), $J_{\mathrm{EQE,bot}}$ is strongly reduced without being able to improve the top current density significantly. It is shown that a front texture with 200 nm $<$ *ACL* $<$ 500 nm reveals a high IRL effectiveness. This is in agreement with [10], where small *ACLs* have been found to be favorable.

B. Finite-Difference Time-Domain Simulation

The most effective solar cells were deposited on textures C, F and G. They show σ_{RMS} and *ACL* values within a certain range. Thus, to achieve a deeper understanding on the individual impact of structure type and feature size on the effectiveness of the IRL, 3-D electromagnetic simulations were carried out. The simulations allow using modified textures with adjusted *ACL*, feature height and consequently the feature steepness. That makes it possible to overcome the experimental limits by the texturing process. For validation, the *EQE* derived from simulations based on the interface textures of type F TCO (LPCVD ZnO:B) are presented exemplarily in Fig. 5. The comparison with measured *EQE* of solar cells deposited on the same front texture shows a higher *EQE* for the top cell, although for the bottom cell, the simulated *EQE* is lower. The effect of the intermediate reflector, maintaining light in the top cell and therefore, reducing the current of the bottom cell, has been successfully reproduced by simulations.

Further, we also carried out simulations on tandem solar cells based on the measured interlayers of type A, C and G TCO. These front textures have been shown to perform in a diverse way and are widely used in research and industry. The results of improvement of $J_{\mathrm{EQE,top}}$ and reduction of $J_{\mathrm{EQE,bot}}$ due to the introduction of an IRL are shown in Fig. 6.

In general, simulated and measured solar cells show similar trends in terms of the $J_{\mathrm{EQE,top}}$-gain and the $J_{\mathrm{EQE,bot}}$-loss. For $J_{\mathrm{EQE,top}}$-gain of solar cells on type A and for $J_{\mathrm{EQE,bot}}$-loss of type C TCO the agreement is excellent. A few differences for bottom solar cells on type F and G are seen. In this series of

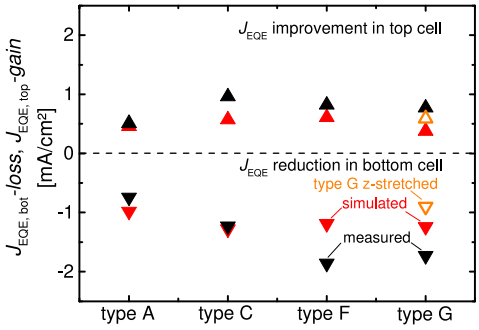

Fig. 6. Comparison between J_{EQE} derived from measurements and simulations of gain in the top cell and loss in the bottom cell for a wavelength range from 500 to 1050 nm. Investigated TCOs are single-textured ZnO:Al (type A), double-textured ZnO:Al (type C), LPCVD ZnO:B (type F), and SnO_2:F (type G). The z-stretched modification of type G TCO is marked by opened orange triangles.

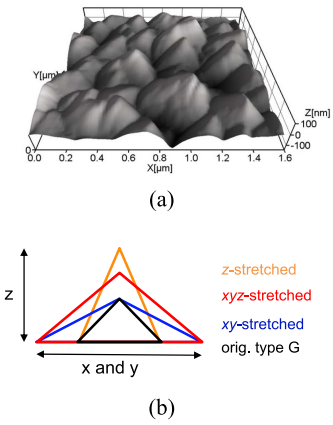

(a)

(b)

Fig. 7. (a) AFM image of a small section of a SnO_2:F (type G) texture. (b) Schematic drawing of different modifications performed for the type G texture by stretching of width and height.

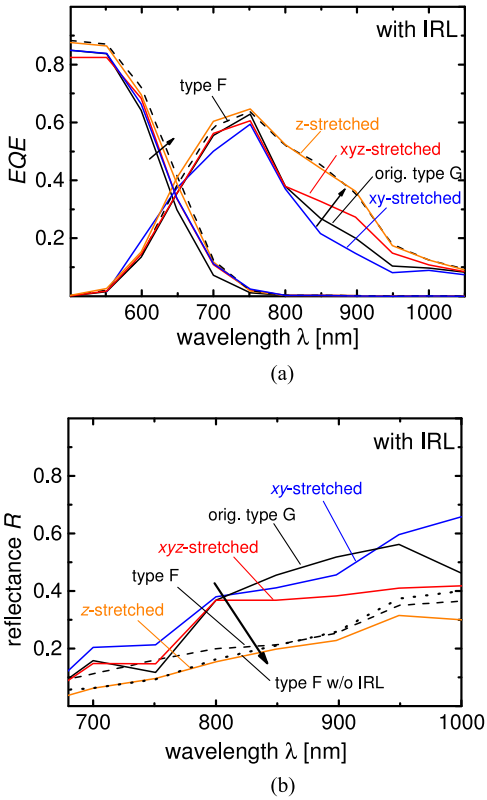

(a)

(b)

Fig. 8. (a) Simulated *EQE* by FDTD of tandem cells with IRL for various stretching modifications based on SnO_2:F (type G) front texture. (b) Simulated reflectance *R* of tandem solar cells with IRL for a wavelength range between 700 and 1000 nm. Simulations using LPCVD ZnO:B (type F) texture (dashed lines) are shown as a reference. Simulated reflectance of a tandem cell without IRL on top of type F textures is shown as a dotted line.

simulations, the difference of the TCO material was not considered. As the TCOs vary not just by texture but also by thickness and refractive index, simulations were carried out holding theses parameters constant and just varying the surface texture. In all simulations, the optical data of ZnO:Al (1%) were used, such that an influence of the TCO material can be seen as a source of error to explain the mismatch between experiment and simulation. Nevertheless, comparing simulated with measured *EQE*s of solar cells shows a sufficiently reliable agreement for various textures.

In the next step, solar cells on a series of artificially stretched textures based on measured SnO_2:F texture (type G) [see Fig. 7 (a)] are simulated. Type G texture was chosen, because tandem cells deposited on top of this TCO show a satisfactory $J_{\mathrm{EQE,top}}$ − gain, but also a high $J_{\mathrm{EQE,bot}}$ − loss. The impact of a stretching of the height of a texture was already previously investigated [13], where the focus was the impact on the improvements in the top cell current. The effects on the bottom current have not been examined before and are presented in the following as simulated *EQE*s.

The differently modified textures are shown in a schematic drawing in Fig. 7 (b). They consist of a lateral stretching (*xy*-stretching), a stretching in three dimensions (*xyz*-stretching), and a stretching only of the height (*z*-stretching). The *xy*-stretching was implemented in a way that the *ACL* of the modified type G texture is equal to ZnO:B (type F). *xyz*-stretching results in a simply enlarged version of type G texture with the same *ACL* and height compared with type F TCO. The third modification is a stretching of height by a factor of 1.5. These modifications allow studying the impact of the lateral structure size and the steepness on the effectiveness of an IRL individually. That way, findings can contribute to the designing of optimized textures for intermediate reflectors.

The stretching was carried out for measurements of the texture at positions i) and iii). For position ii), we applied the nonconformal growth model described in [22] on the stretched texture from position i). Results of the simulated *EQE*s of tandem cells with IRL by FDTD for stretching modifications of type G TCO are shown in Fig. 8(a). Very pronounced effects are observed in the bottom cells. The *xy*-stretching causes a flattening of the texture and leads to a decrease of bottom cell *EQE* compared with the original texture of type G TCO. The *xyz*-stretching, however, improves the *EQE* in the bottom cell, which is due to a better scattering of light at larger wavelengths. Finally, the most pronounced effects are observed for the *z*-stretched texture. Top and bottom cell *EQE*s on this modification of type G TCO are increased and even exceed the *EQE*s of solar cells deposited on

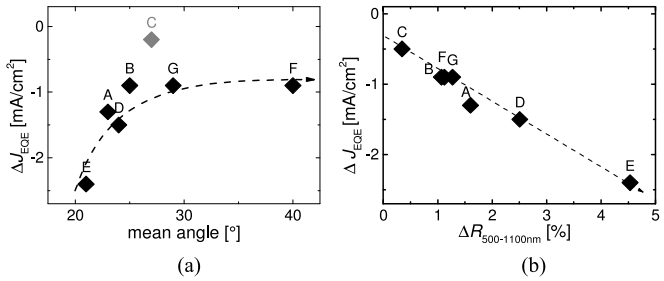

Fig. 9. (a) ΔJ_{EQE} shown as a function of mean angle of the angular distribution derived from AFM data. (b) Correlation between measured ΔJ_{EQE} and ΔR (difference between cell reflection of tandem cells with and without IRL) for tandem cells deposited on TCOs type A–H for a wavelength range from 500 to 1100 nm. Dashed lines are a guide for the eye.

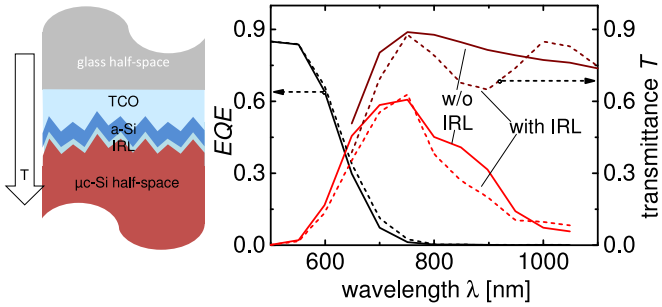

Fig. 10. Simulated transmittance (brown lines) from a top cell into a silicon half-space (see schematic) as a comparison with the simulated bottom cell *EQE* (red lines). Dashed lines indicate the presence of an IRL. For simulations, SnO_2:F (type G) textures were applied.

type F TCO (ZnO:B). The improvements compared with unmodified type G TCO in terms of short-circuit current density are presented in Fig. 6. The simulated solar cell reflectance is shown in Fig. 8(b). As compared with the *EQE*, a strong dependence between the modified structures and the optical effects is seen. In the same way as the *EQE* is increased for the *z*-stretched structures, a strong decrease of the reflectance is observed. In turn, the flattened *xy*-stretched structures show an enhanced cell reflectance, which is also congruent to the *EQE* results. In early studies, it has already been predicted that the total current is correlated to the cell reflection [11], while the influence to the bottom current losses are not correlated to the variation of the texture. Experimental and simulated data shown in Figs. 4(b) and 8 indicate that parasitic reflection of light from the IRL out of the solar cell is mainly responsible for the loss of bottom cell current, when comparing tandem cells with and without IRL. In this respect, the steepness of the texture is the most relevant measure. The same effect is found for the experimental data.

In Fig. 9(a), ΔJ_{EQE} is shown as a function of mean angle from the angular distribution derived from AFM data. It reveals that ΔJ_{EQE}, a parameter to describe the loss caused by the IRL, is improved with larger structure angles. It should be mentioned that the limiting AFM resolutions could not resolve the very small and steep craters in double-textured ZnO:Al (type C) fully and therefore, the true mean angle value of type C might be larger than displayed in the graph. In Fig. 9(b), the dependence between ΔJ_{EQE} and $\Delta R_{500-1100\,\mathrm{nm}}$, the difference between cell reflectance of tandem cells with and without IRL for a wavelength range from 500 to 1100 nm is shown. A linear correlation for textured TCO types A–G is observed. Type C TCO, the texture with the lowest ΔJ_{EQE} also shows almost no additional reflection when an IRL is introduced. Accordingly, textures with high ΔJ_{EQE} also reveal large values for $\Delta R_{500-1100\,\mathrm{nm}}$. High losses found for solar cells deposited on flatter textures reveal large parasitic reflection by introducing an IRL. This is due to the increased amount of light, which is reflected in an angle smaller than the angle of total reflection and, therefore, is not trapped within the solar cell.

To distinguish the reflection effects caused by the IRL and the back reflector, transmittance after the top cell and IRL are simulated for the case in which the bottom cell is substituted by a silicon half-space (see Fig. 10). Here, the transmittance agrees with the *EQE*. It shows that the effect of the reduced *EQE* is in fact due to reflection losses from the IRL and not from the back reflector.

In this contribution, we have found that a higher steepness will lead to a higher effectiveness of the IRL. At the same time, very steep structures might be companioned with a decrease of voltage. The V_{oc} for solar cells deposited on type C TCO reveals the lowest value compared with other textures. A smoothing of the IRL would be beneficial to the V_{oc} and *FF*, as seen in [23], and a tradeoff between optical and electrical effects has to be taken into account.

IV. Conclusion

In this contribution, we have investigated the interplay between the TCO topography and the performance of the intermediate reflector in thin-film silicon tandem solar cells. Differences in terms of morphology, light scattering, and effectiveness of the IRL were observed. Experimental results show that the best performances were achieved with front textures with an *ACL* between 200 and 500 nm. The best IRL performance was found for double-textured ZnO:Al. Compared with single-textured ZnO:Al, the *ACL* is smaller, and the feature steepness is higher. A reduced cell reflectance improves the effectiveness of IRL, as well as the conversion efficiency of the solar cell.

Three-dimensional electromagnetic simulations reproduced the *EQE* of tandem solar cells and rendered possible the investigation of systematically modified structures, i.e., the steepening of the texture shows an enhancement of top cell current and a significant reduction of current loss in the bottom cell after application of the IRL layer in tandem solar cells. This is linked to a reduction of parasitic reflection. We have shown that for the design of an optimized texture, steeper structures are preferred in terms of light management for both subcells in tandem solar cells.

Acknowledgment

The authors would like to thank U. Rau for his continuous support and helpful discussions. They would also like to thank J. Kirchhoff, U. Gerhards, and S. Kasper for solar cell deposition and characterization and Neuchatel IMT for provision of the ZnO:B substrates.

REFERENCES

[1] D. L. Staebler and C. R. Wronski, "Reversible conductivity changes in discharge-produced amorphous Si," *Appl. Phys. Lett.*, vol. 31, pp. 292–294, 1977.

[2] B. Rech and H. Wagner, "Potential of amorphous silicon for solar cells," *Appl. Phys. A: Mater. Sci. Process.*, vol. 69, no. 2, pp. 155–167, 1999.

[3] K. Yamamoto, A. Nakajima, M. Yoshimi, T. Sawada, S. Fukuda, T. Suezaki, M. Ichikawa, Y. Koi, M. Goto, T. Meguro, T. Matsuda, M. Kondo, T. Sasaki, and Y. Tawada, "A high efficiency thin film silicon solar cell and module," *Sol. Energy*, vol. 77, no. 6, pp. 939–949, 2004.

[4] P. Buehlmann, J. Bailat, D. Dominé, A. Billet, F. Meillaud, A. Feltrin, and C. Ballif, "*In situ* silicon oxide based intermediate reflector for thin-film silicon micromorph solar cells," *Appl. Phys. Lett.*, vol. 91, pp. 143505-1–143505-3, 2007.

[5] A. Lambertz, T. Grundler, and F. Finger, "Hydrogenated amorphous silicon oxide containing a microcrystalline silicon phase and usage as an intermediate reflector in thin-film silicon solar cells," *J. Appl. Phys.*, vol. 109, pp. 113109-1–113109-11, 2011.

[6] P. Cuony, D. T. L. Alexander, I. Perez-Wurfl, M. Despeisse, G. Bugnon, M. Boccard, T. Söderström, A. Hessler-Wyser, C. Hébert, and C. Ballif, "Silicon filaments in silicon oxide for next-generation photovoltaics," *Adv. Mater.*, vol. 24, no. 9, pp. 1182–1186, 2012.

[7] A. Lambertz, V. Smirnov, T. Merdzhanova, K. Ding, S. Haas, G. Jost, R. Schropp, F. Finger, and U. Rau, "Microcrystalline silicon–oxygen alloys for application in silicon solar cells and modules," *Sol. Energy Mater. Sol. Cells*, vol. 119, pp. 134–143, 2013.

[8] P. Obermeyer, C. Haase, and H. Stiebig, "Advanced light trapping management by diffractive interlayer for thin-film silicon solar cells," *Appl. Phys. Lett.*, vol. 92, no. 18, pp. 181102-1–181102-3, 2008.

[9] C. Rockstuhl, F. Lederer, K. Bittkau, T. Beckers, and R. Carius, "The impact of intermediate reflectors on light absorption in tandem solar cells with randomly textured surfaces," *Appl. Phys. Lett.*, vol. 94, pp. 211101-1–211101-3, 2009.

[10] S. Kirner, M. Hammerschmidt, C. Schwanke, D. Lockau, S. Calnan, T. Frijnts, S. Neubert, A. Schopke, F. Schmidt, J.-H. Zollondz, A. Heidelberg, B. Stannowski, B. Rech, and R. Schlatmann, "Implications of TCO topography on intermediate reflector design for a-si/μc-si tandem solar cells—Experiments and rigorous optical simulations," *IEEE J. Photovoltaics*, vol. 4, no. 1, pp. 10–15, Jan. 2014.

[11] N. Pellaton Vaucher, J.-L. Nagel, R. Platz, D. Fischer, and A. Shah, "Light management in tandem cells by an intermediate reflector layer," in *Proc. 2nd World Conf. Photovoltaic Energy Convers.*, 1998, pp. 728–731.

[12] D. Domine, J. Bailat, J. Steinhauser, and A. Shah, "Micromorph solar cell optimization using a ZnO layer as intermediate reflector," in *Proc. 4th World Conf. Photovoltaic Energy Convers.*, 2006, pp. 1465–1468.

[13] C. Rockstuhl, S. Fahr, K. Bittkau, T. Beckers, R. Carius, F.-J. Haug, T. Söderström, C. Ballif, and F. Lederer, "Comparison and optimization of randomly textured surfaces in thin-film solar cells," *Opt. Exp.*, vol. 18, pp. A335–A341, 2010.

[14] A. Čampa, M. Meier, M. Boccard, L. V. Mercaldo, M. Ghosh, C. Zhang, T. Merdzhanova, J. Krč, F.-J. Haug, and M. Topič, "Micromorph silicon solar cell optical performance: Influence of intermediate reflector and front electrode surface texture," *Sol. Energy Mater. Sol. Cells*, vol. 130, pp. 401–409, 2014.

[15] C. Zhang, M. Meier, A. Lambertz, V. Smirnov, B. Holländer, A. Gordijn, and T. Merdzhanova, "Optical and electrical effects of p-type μc-SiOx:H in thin-film silicon solar cells on various front textures," *Int. J. Photoenergy*, vol. 2014, no. 1–2, pp. 1–10, 2014.

[16] O. Kluth, B. Rech, L. Houben, S. Wieder, G. Schöpe, and C. Beneking, "Texture etched ZnO:Al coated glass substrates for silicon based thin film solar cells," *Thin Solid Films*, vol. 351, no. 1–2, pp. 247–253, 1999.

[17] S. Faÿ, L. Feitknecht, R. Schlüchter, U. Kroll, E. Vallat-Sauvain, and A. Shah, "Rough ZnO layers by LP-CVD process and their effect in improving performances of amorphous and microcrystalline silicon solar cells," *Sol. Energy Mater. Sol. Cells*, vol. 90, no. 18–19, pp. 2960–2967, 2006.

[18] J. I. Owen, J. Hüpkes, H. Zhu, E. Bunte, and S. E. Pust, "Novel etch process to tune crater size on magnetron sputtered ZnO:Al," *Phys. Stat. Sol.*, vol. 208, pp. 109–113, 2011.

[19] A. F. Oskooi, D. Roundy, M. Ibanescu, P. Bermel, J. D. Joannopoulos, and S. G. Johnson, "MEEP: A flexible free-software package for electromagnetic simulations by the FDTD method," *Comput. Phys. Commun.*, vol. 181, pp. 687–702, 2010.

[20] A. Hoffmann, K. Bittkau, C. Zhang, T. Merdzhanova, and U. Rau, "Coupling incident light to guided modes in thin-film tandem solar cells with intermediate reflector," *IEEE J. Photovoltaics*, 2014, DOI:10.1109/JPHOTOV.2014.2359740.

[21] G. Jost, T. Merdzhanova, J. I. Owen, T. Zimmermann, and J. Hüpkes, "Front contact texture optimization for a-si:h/μc-si:h tandem solar cells," *Prog. Photovoltaics: Res. Appl.*, 2014.

[22] M. Sever, B. Lipovšek, J. Krč, A. Čampa, G. Sánchez Plaza, F.-J. Haug, M. Duchamp, W. Soppe, and M. Topič, "Combined model of non-conformal layer growth for accurate optical simulation of thin-film silicon solar cells," *Sol. Energy Mater. Sol. Cells*, vol. 119, pp. 59–66, 2013.

[23] M. Boccard, C. Battaglia, N. Blondiaux, R. Pugin, M. Despeisse, and C. Ballif, "Smoothening intermediate reflecting layer for tandem thin-film silicon solar cells," *Sol. Energy Mater. Sol. Cells*, vol. 119, pp. 12–17, 2013.

Authors' photographs and biographies not available at the time of publication.